

Supporting Information

Jafar-Nejad et al. 10.1073/pnas.1018748108

SI Experimental Procedures

Column Fractionation and Analysis. Gel filtration chromatography was carried out at 4 °C using a General Electric AKTA PURIFIER FPLC system. Cerebellar or HEK293T-cell extracts were prepared fresh, and 700 μ L was loaded for FPLC. Gel filtration was done using a Superose 6 10/300 GL column (General Electric) equilibrated in TST buffer [50 mM Tris (pH 8), 50 mM NaCl, 0.5% Triton 100X] at 0.3 mL/min. Fractions were collected in 1-mL increments. The column void volume is 6.73 mL (fraction 7), and elution volumes of gel filtration standards are 11.66 mL (fraction 12) for thyroglobulin (669 kDa), 14.78 mL (fraction 15) for alcohol dehydrogenase (150 kDa), and 18.24 mL (fraction 19) for cytochrome C (12.4 kDa). Fractions were supplemented with protease inhibitors and immediately prepared for SDS/PAGE.

Quantification of Dendritic Arborization and Purkinje Cell Loss. Lines (250 μ m) were drawn from the Purkinje cell soma center to the soma center along the length of the Purkinje cell layer visible in

the optical section. Purkinje cells were identified using a calbindin image mask created as described above (using a defined constant setting for all images). Fluorescence intensity was measured from soma of Purkinje cells to the end of the adjacent molecular layer for cells in which the central nucleus was clearly visible. The number of Purkinje cells per 250 μ m was calculated by dividing the number of cells by the length of the Purkinje cell layer measured in each optical section.

Breathing Measurements. To identify intervals of calm breathing, a pilot study was performed in which breathing frequency was compared across calm and active states using a threshold of 500 breaths per minute. Less than 10% of recorded breaths during “calm” minutes occurred at frequencies of over 500 breaths per minute, whereas more than 10% of recorded breaths were above this threshold in “active” minutes, which corresponded with rapid sniffing behavior. Thus, only minutes with less than 10% of recorded breaths above a rate of 500 breaths per minute were included and yielded results similar to behavioral monitoring.

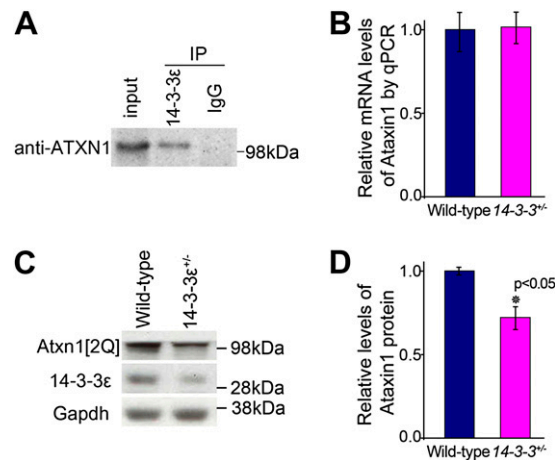


Fig. S1. 14-3-3 ϵ stabilizes ATXN1 in vivo. (A) Anti-14-3-3 ϵ antibody coimmunoprecipitated ATXN1 from WT mouse cerebellar extract. (B) Quantitative RT-PCR of cerebellar ATXN1 mRNA in 14-3-3 $\epsilon^{-/-}$ mice compared with WT littermates ($n = 3$). (C) Western blot for 14-3-3 ϵ , WT ATXN1 (ATXN1[2Q]), and the control Gapdh in cerebellar lysates. (D) Quantification of Western blot in C. The level of endogenous ATXN1 is reduced in 14-3-3 $\epsilon^{-/-}$ relative to levels in WT extracts ($n = 6$).

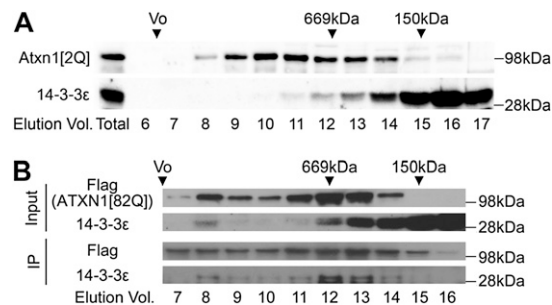


Fig. S2. 14-3-3 ϵ interacts with ATXN1 in its large protein complexes. (A) Representative Western blots of 1-mL gel filtration fractions of WT mouse cerebellar extract analyzed for ATXN1 and 14-3-3 ϵ . (B) Representative Western blots of gel filtration fractions of HEK293T cells transfected with Flag-ATXN1[82Q], analyzed for Flag-ATXN1[82Q] and endogenous 14-3-3 ϵ , and immunoprecipitated (IP) from each fraction with anti-FLAG antibody.

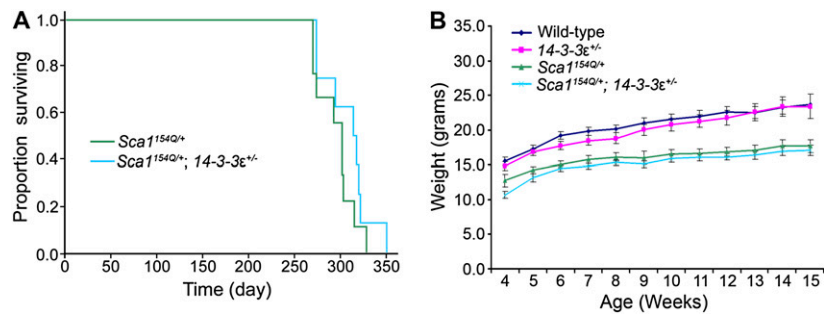


Fig. S3. (A) Age of death for *Sca1*^{154Q/+} ($n = 10$) and *Sca1*^{154Q/+}; *14-3-3ε*^{-/-} ($n = 11$) animals. The Kaplan-Meier survival curve shows that *14-3-3ε* haploinsufficiency does not affect the life span of *Sca1*^{154Q/+} mice. (B) *14-3-3ε* haploinsufficiency did not alter the average weight (\pm SEM) of different genotypes (indicated by color) plotted weekly from 4 to 15 wk of age.

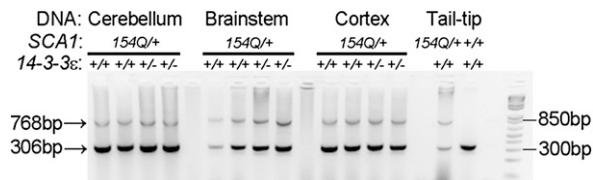


Fig. S4. PCR analysis was performed on cerebellum, brainstem, and cortex from two *Sca1*^{154Q/+} and two *Sca1*^{154Q/+}; *14-3-3ε*^{-/-} mice along with tail-tip DNA from a *Sca1*^{154Q/+} mouse and a WT mouse. The reaction gives 306 bp for the WT allele and 768 bp for the *Sca1*^{154Q} allele.

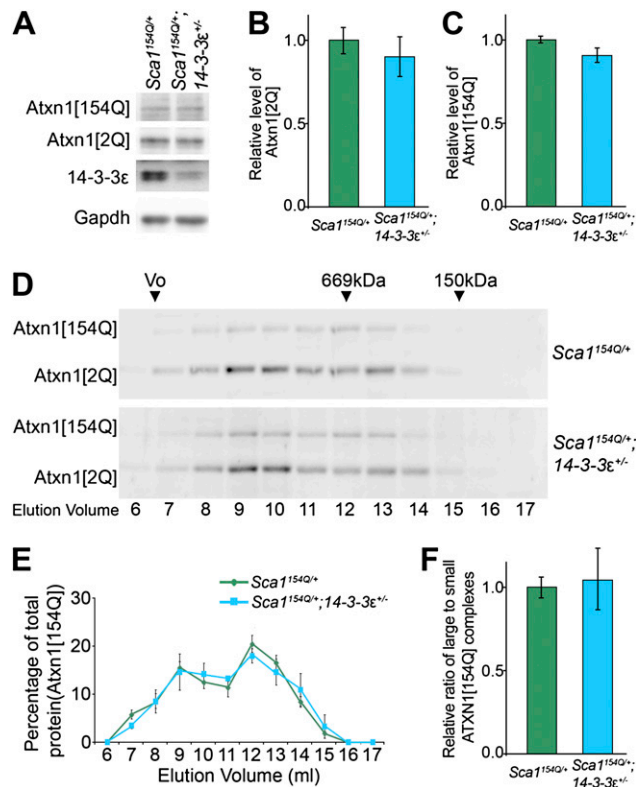


Fig. S5. *14-3-3ε* haploinsufficiency affects neither the levels nor distributions of the WT and expanded ATXN1 extracted from the brainstem. (A–C) SDS/PAGE of mouse brainstem extracts (genotypes indicated) analyzed by Western blotting for *14-3-3ε*, ATXN1 (2Q and 154Q), and the control *Gadph*. The average level (\pm 95% confidence interval) of ATXN1[2Q] and ATXN1[154Q] proteins in *Sca1*^{154Q/+}; *14-3-3ε*^{-/-} extracts relative to levels in *Sca1*^{154Q/+} extracts is illustrated in *B* and *C*, respectively ($n = 3$). Unlike the cerebellum, *14-3-3ε* haploinsufficiency does not displace ATXN1[154Q] from its larger complexes in the brainstem. (D) Representative proteins from size exclusion chromatography fractions of mouse brainstem extracts analyzed for ATXN1[2Q] and ATXN1[154Q]. (E) ATXN1 [154Q] gel filtration elution profiles of brainstem extracts plotted as the percentage of ATXN1[154Q] (mean \pm SEM) in each fraction (amount per fraction compared with total amount of ATXN1[154Q] in all fractions) from independent extracts ($n = 3$). (F) Large (in the peak elution fractions, 9 and 10 mL) to small (12 and 13 mL) ATXN1[154Q] complexes are present in these extracts ($n = 3$).

